Available online at www.sciencedirect.com
ScienceDirect
International Journal of Thermal Sciences 47 (2008) 237–248
International Journal of Thermal Sciences
www.elsevier.com/locate/ijts

Numerical simulation of double diffusive natural convection in rectangular enclosure in the presences of magnetic field and heat source

Mohamed A. Teamah

Mechanical Engineering Department, Alexandria University, Alexandria, Egypt

Received 19 August 2006; received in revised form 4 February 2007; accepted 4 February 2007

Available online 29 March 2007

Abstract

Double-diffusive convective flow in a rectangular enclosure with the upper and lower surfaces being insulated and impermeable is studied numerically. Constant temperatures and concentration are imposed along the left and right walls of the enclosure. In addition, a uniform magnetic field is applied in a horizontal direction. Laminar regime is considered under steady state condition. The transport equations for continuity, momentum, energy and spices transfer are solved. The numerical results are reported for the effect of thermal Rayleigh number, heat generation or absorption coefficient and the Hartmann number on the contours of streamline, temperature, and concentration as well as the dimensionless density. In addition, the predicted results for the average Nusselt and Sherwood numbers are presented and discussed for various parametric conditions. This study was done for constant aspect ratio $A = 2$, Lewis number $Le = 1$ and Prandtl number $Pr = 0.7$. The study covers ranges for $10^3 \leqslant Ra_T \leqslant 10^6$, $0 \leqslant Ha \leqslant 200$, $-50 \leqslant \phi \leqslant 25$ and $-10 \leqslant N \leqslant 10$.

Keywords: Double-diffusive flow; Heat and mass transfer; Magnetic field; Heat generation; Heat absorption; Numerical solution

1. Introduction

Natural convection is of a great importance in many industrial applications. Convection plays a dominant role in crystal growth in which it affects the fluid-phase composition and temperature at the phase interface. It is the foundation in modern electronics industry to produce pure and perfect crystals to make transistors, lasers rods, microwave devices, infrared detectors, memory devices, and integrated circuits. Natural convection adversely affects local growth conditions and enhances the overall transport rate. In addition, the application of a magnetic field in various research areas has significantly increased in recent years. The development of super-conducting magnets has allowed the generation of magnetic fields up to 20 T (or higher with hybrid magnets), as reported by Ujihara et al. [1].

Many investigators studied the simple rectangular and square cavities with temperature gradient experimentally and numerically. A good review was reported by Ostrach [2]. A complicated inclined cavity with inner heat generation was studied numerically by Acharya and Goldstein [3]. They introduced two Rayleigh numbers. The first is internal Rayleigh Ra_I, based on the rate of heat generation and external Rayleigh number Ra_E, based on temperature difference. Their study covered a range for Ra_I from 10^4 to 10^7 and Ra_E from 10^3 to 10^6, and cavity inclination angle from 30° to 90°. Also, Rahman and Sharif [4] studied numerically the same geometry with heated bottom and cooled top surfaces and insulated sides. In their study, both Ra_I and Ra_E were 2×10^5 and the aspect ratio ranged from 0.25 to 4. They found that for $Ra_E/Ra_I > 1$, the convective flow and heat transfer were almost the same as that in a cavity without internal heat generating fluid and they observed similar results as in Acharya and Goldstein [3]. Oztop and Bilgen [5] studied numerically the presence of a partial divider in a differentially heated enclosure containing heat generating fluid which adds an additional dynamic effect to overall convection characteristics. Their study covered both Ra_I and Ra_E over a range from 10^3 to 10^6. Also, they studied the various partial divider geometry and position. In their study they used a modified version of the general-purpose SAINTS software (Software for Arbitrary Integration of Navier–Stokes Equation with a Turbulence and

E-mail address: mteamah@yahoo.com.

1290-0729/$ – see front matter
doi:10.1016/j.ijthermalsci.2007.02.003

Nomenclature

A	aspect ratio, H/L	
B_o	magnetic induction	Tesla = N/A m^2
c	vapour concentration	
c_h	concentrations at the left wall of the cavity	
c_l	concentrations at the right wall of the cavity	
C	dimensionless vapour concentration, $C = (c - c_l)/(c_h - c_l)$	
D	mass diffusivity	m^2/s
g	acceleration of gravity	m/s^2
Gr_S	solutal Grashof number	
Gr_T	thermal Grashof number	
h	heat transfer coefficient	W/m^2 K
h_s	solutal transfer coefficient	m/s
H	cavity height	m
Ha	Hartmann number, $B_o L\sqrt{\sigma/\mu}$	
k	fluid thermal conductivity	W/m K
L	cavity width	m
Le	Lewis number, $Le = \alpha/D = Sc/Pr$	
N	buoyancy ratio	
Nu	average Nusselt number, $Nu = hL/k$	
Nu_i	local Nusselt number	
p	pressure	N/m^2
P	dimensionless pressure, $P = pH_o^2/\rho_o\alpha^2$	
Pr	Prandtl number, $Pr = \nu/\alpha$	
Q_o	heat generation or absorption coefficient	W/m^3 °C
Ra_S	solutal Rayleigh number, $Ra_S = Gr_S^* Pr$	
Ra_T	thermal Rayleigh number, $Ra_T = Gr_T^* Pr$	
Sc	Schmidt number, $Sc = \nu/D$	
Sh	average Sherwood number, $Sh = h_s L/D$	
Sh_i	local Sherwood number	
T	local temperature	K
T_c	cold wall temperature	K
T_h	hot wall temperature	K
ΔT	temperature difference, $T_h - T_c$	K
u	velocity components in x direction	
v	velocity components in y direction	
U	dimensionless velocity component in X direction	
V	dimensionless velocity component in Y direction	
x, y	dimensional coordinates	
X, Y	dimensionless coordinates	

Greek symbols

α	thermal diffusivity	m^2/s
β_T	coefficient of thermal expansion	K^{-1}
β_S	coefficient of solutal expansion	m^3/kg
ϕ	dimensionless heat generation or absorption	
θ	dimensionless temperature, $(T - T_c)/(T_h - T_c)$	
μ	dynamic viscosity	kg/m s
ν	kinematics viscosity	m^2/s
ρ	local fluid density	kg/m^3
ρ_o	fluid density at the bottom surfaces	kg/m^3
ρ^*	dimensionless density $= NC - \theta$	
σ	electrical conductivity	A m/V
Ψ	dimensionless stream function	
$\Psi_{\max}$	maximum dimensionless stream function	

Porous Media Simulator). SAINTS makes use of the SIMPLE algorithm explained by Patankar [6].

One of the effective means practiced in industry for thermally induced melt flow control is magnetic damping, which is derived from the interaction between an electrically conducting melt flow and an applied magnetic field to generate an opposing Lorentz force to the convective flows in the melt. The damping effect depends on the strength of the applied magnetic field and its orientation with respect to the convective flow direction. Substantial theoretical and numerical work, thus far, has appeared on magnetic damping for natural convection as reported by Shu et al. [7]. Ozoe and Okada [8] conducted a numerical analysis of the magnetic damping effect in a cubic cavity with two vertical walls at different temperatures. They found that the strongest damping effect is achieved with the magnetic field applied perpendicular to the hot wall. This is consistent with the work of Alboussière et al. [9] who used an asymptotic approach, and found that for a rectangular box, the damping effect is the weakest when the applied magnetic field is horizontal and parallel to the hot wall. Wakayama [10] reported a jet flow of nitrogen gas in a decreasing magnetic field as another example of this magnetic force. Bai et al. [11] made a numerical analysis for this study. Tagawa et al. [12] employed a similar way to Boussinesq approximation for this magnetic force and carried out numerical analysis for natural convection of air in a cubic enclosure. Kaneda et al. [13] studied the natural convection in a cube enclosure filled with air. The cube was heated from above and cooled from bottom and the air was driven by a magnetic force. Xu et al. [14] studied experimentally the thermally induced convection of molten gallium in magnetic fields.

During the magnetic liquid encapsulated Czochralski (MLEC) growth of compound semiconductor crystals, a single-crystal seed is lowered through the encapsulate which initiates solidification and crystal growth begins in the presence of an externally applied magnetic field. Morton et al. [15] presented a model of dopant transport during the MLEC process. Previous researchers have investigated the effect of a steady magnetic field on two-dimensional natural convection in rectangular enclosures. Ma and Walker [16,17] conducted a model of dopant transport during Bridgman crystal growth with magnetically damped buoyant convection and followed it by a parametric study of segregation effects during vertical Bridgman crystal growth with an axial magnetic field. Kuniholm and Ma [18] used an asymptotic analysis in order to investigate the interaction between the melt and the encapsulant in a rectangular enclosure with strong magnetic fields. Yang and Ma [19] studied natural convection in a liquid encapsulated molten semiconductor with a horizontal magnetic field numerically. Recently,

Wang and co-workers [20–24] conducted very strong series of numerical researches in different methods of crystal growth with electric and magnetic fields in alloys manufacture.

Nishimura et al. [25] studied numerically the oscillatory double-diffusive convection in a rectangular enclosure with combined horizontal temperature and concentration gradients. They concluded that the oscillatory double-diffusive convection with the secondary cell flow structure occurs for a certain range of buoyancy ratio from $N = 1.044$ to 1.122. Chamkha and Al-Naser [26] studied numerically the hydromagnetic double-diffusive convection in a rectangular enclosure with opposing temperature and concentration gradients. Their cavity and conditions were similar to that of Nishimura [25] but they imposed magnetic field and heat generation. They found that the effect of the magnetic field reduced the heat transfer and fluid circulation within the enclosure. Also, they concluded that the average Nusselt number increased owing to the presence of a heat sink while it decreased when a heat source was present. And they reported that the periodic oscillatory behavior in the stream function inherent in the problem was decayed by the presence of the magnetic field. This decay in the transient oscillatory behavior was speeded up by the presence of a heat source. Chamkha and Al-Naser [27] extended their previous work by changing the boundary conditions of vertical walls to be at constant heat and mass fluxes.

This study is a parametric study and extension for Chamkha and Al-Naser [26,27] study. A wide range for thermal Rayleigh number is studied from 10^3 to 10^6. This range covers most of the engineering and industrial applications. In addition, a strong magnetic field required for modern electronic devices is considered in this study. For this reason the Hartmann number is increased to 200. Also, the heat generation and absorption coefficients range from -50 to $+25$. Moreover, the buoyancy ratio varied from -10 to $+10$.

2. Mathematical model

The schematic of the system under consideration is shown in Fig. 1. The temperatures T_h and T_c are uniformly imposed along the vertical walls. The top and bottom surfaces are assumed to be adiabatic and impermeable. The left wall is the source for both heat and mass. A magnetic field with uniform strength B_0 is applied in the horizontal direction. Also, the enclosure is filled with a binary mixture of gas. The fluid is assumed to be incompressible, Newtonian, heat generating or absorbing and viscous. Both the viscous dissipation and magnetic dissipation are assumed to be negligible. The magnetic Reynolds number is assumed to be so small that the induced magnetic field is neglected. The Boussinesq approximation equation (1) with opposite and compositional buoyancy forces is used for the body force terms in the momentum equations.

$$\rho = \rho_o\left[1 - \beta_T(T - T_c) - \beta_S(c - c_l)\right] \tag{1}$$

The governing equations for the problem under consideration are based on the balance laws of mass, linear momentum, thermal energy and concentration in two dimensions steady

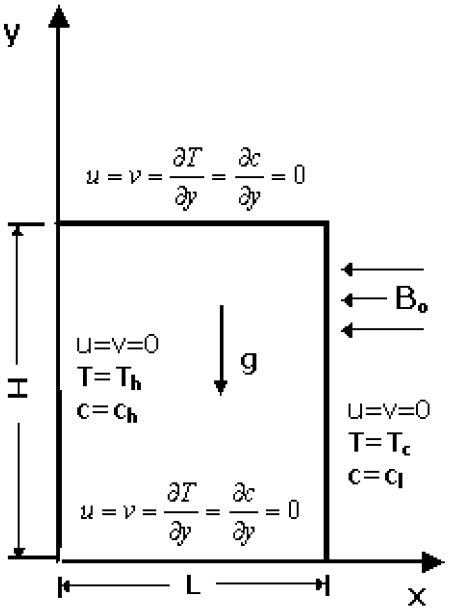

Fig. 1. A schematic diagram for the problem with boundary conditions.

state. Following the previous assumptions, these equations can be written in dimensional form as:

$$\frac{\partial u}{\partial x} + \frac{\partial v}{\partial y} = 0 \tag{2}$$

$$u\frac{\partial u}{\partial x} + v\frac{\partial u}{\partial y} = -\frac{1}{\rho}\frac{\partial p}{\partial x} + \upsilon\left[\frac{\partial^2 u}{\partial x^2} + \frac{\partial^2 u}{\partial y^2}\right] \tag{3}$$

$$u\frac{\partial v}{\partial x} + v\frac{\partial v}{\partial y} = -\frac{1}{\rho}\frac{\partial p}{\partial y} + \upsilon\left[\frac{\partial^2 v}{\partial x^2} + \frac{\partial^2 v}{\partial y^2}\right] + g\beta_T(T - T_c) - g\beta_c(c - c_l) + \frac{\sigma B_o^2}{\rho}v \tag{4}$$

$$u\frac{\partial T}{\partial x} + v\frac{\partial T}{\partial y} = \alpha\left[\frac{\partial^2 T}{\partial x^2} + \frac{\partial^2 T}{\partial y^2}\right] + \frac{Q_o}{\rho C_p}(T - T_c) \tag{5}$$

$$u\frac{\partial c}{\partial x} + v\frac{\partial c}{\partial y} = D\left[\frac{\partial^2 c}{\partial x^2} + \frac{\partial^2 c}{\partial y^2}\right] \tag{6}$$

Where B_o is the magnetic induction vector in Tesla, σ is the electrical conductivity, A m/V, Q_o, heat generation or absorption coefficient, W/m^3 °C, and D is the mass diffusivity, m^2/s. The boundary conditions are:

- $u = v = 0.0$, $T = T_h$ and $c = c_h$, at $x = 0$,
- $u = v = 0.0$, $T = T_c$ and $c = c_l$, at $x = L$

and at $y = 0$ and $y = H$

$$u = v = \frac{\partial T}{\partial y} = \frac{\partial c}{\partial y} = 0$$

And introducing the following dimensionless groups for the governing equations,

$$X = \frac{x}{L}, \quad Y = \frac{y}{L}, \quad U = \frac{uL}{\alpha}, \quad V = \frac{vL}{\alpha}, \quad P = \frac{pL^2}{\rho_o^*\alpha^2}$$

$$\theta = \frac{T - T_c}{T_h - T_c} \quad \text{and} \quad C = \frac{c - c_l}{c_h - c_l} \tag{7}$$

A set of governing equations is obtained as:

$$\frac{\partial U}{\partial X}+\frac{\partial V}{\partial Y}=0 \tag{8}$$

$$U\frac{\partial U}{\partial X}+V\frac{\partial U}{\partial Y}=-\frac{\partial P}{\partial X}+Pr\left[\frac{\partial^2 U}{\partial X^2}+\frac{\partial^2 U}{\partial Y^2}\right] \tag{9}$$

$$U\frac{\partial V}{\partial X}+V\frac{\partial V}{\partial Y}=-\frac{\partial P}{\partial Y}+Pr\left[\frac{\partial^2 V}{\partial X^2}+\frac{\partial^2 V}{\partial Y^2}\right]+Ra_T Pr[\theta-NC]+Ha^2 Pr\times V \tag{10}$$

$$U\frac{\partial \theta}{\partial X}+V\frac{\partial \theta}{\partial Y}=\left[\frac{\partial^2 \theta}{\partial X^2}+\frac{\partial^2 \theta}{\partial Y^2}\right]+\phi\times\theta \tag{11}$$

$$U\frac{\partial C}{\partial X}+V\frac{\partial C}{\partial Y}=\frac{1}{Le}\left[\frac{\partial^2 C}{\partial X^2}+\frac{\partial^2 C}{\partial Y^2}\right] \tag{12}$$

Where, Pr is the Prandtl number, Ra_T is the thermal Rayleigh number, N is the buoyancy ratio $=[\beta_s(c_h-c_l)]/[\beta_T(T_h-T_c)]$, Ha is the Hartmann number $=B_oL\sqrt{\sigma/\mu}$, Φ is the dimensionless heat generation or absorption coefficient $=(Q_oL^2)/(\rho c_p\alpha)$, and Le is the Lewis number.

The dimensionless boundary conditions are:

- $U=V=0.0$, $\theta=1$ and $C=1$, at $X=0$,
- $U=V=\theta=C=0.0$, at $X=1$.

And at $Y=0$ and at $Y=$ aspect ratio

$$U=V=\frac{\partial\theta}{\partial Y}=\frac{\partial C}{\partial Y}=0 \tag{13}$$

2.1. Nusselt number calculation

Equating the heat transfer by convection to the heat transfer by conduction at hot wall:

$$h\Delta T=-k\left(\frac{\partial T}{\partial x}\right)_{x=0} \tag{14}$$

Introducing the dimensionless variables, defined in Eq. (7), into Eq. (14), gives:

$$Nu_l=-\left(\frac{\partial\theta}{\partial X}\right)_{X=0} \tag{15}$$

The average Nusselt number is obtained by integrating the above local Nusselt number over the vertical wall:

$$Nu=-\frac{1}{A}\int_0^A\left(\frac{\partial\theta}{\partial X}\right)_{X=0}\mathrm{d}Y \tag{16}$$

2.2. Sherwood number calculation

Equating the extracted mass transfer by convection to the added mass transfer to the cavity gives:

$$h_s\Delta c=-D\left(\frac{\partial c}{\partial x}\right)_{x=0} \tag{17}$$

Introducing the dimensionless variables, defined in Eq. (7), into Eq. (14), gives:

$$Sh_l=-\left(\frac{\partial C}{\partial X}\right)_{X=0} \tag{18}$$

The average Sherwood number is obtained by integrating the above local Sherwood number over the vertical wall:

$$Sh=-\frac{1}{A}\int_0^A\left(\frac{\partial C}{\partial X}\right)_{X=0}\mathrm{d}Y \tag{19}$$

3. Solution procedure

The governing equations were solved using the finite volume technique developed by Patankar [6]. This technique was based on the discretization of the governing equations using the central difference in space. Firstly, the number of nodes used was checked. The deviations between the results obtained for domain (22×62) and (82×242) were less than 0.15%. Therefore, throughout this study, the number of grids (42×122) was used. The 42 grid points in X-direction were enough to resolve the thin boundary layer near the vertical walls. To calculate both Nusselt and Sherwood numbers, we use numerical differentiations, $(\partial\theta/\partial X)_{X=0}$ and $(\partial\theta/\partial X)=\mathrm{Lim}_{\Delta X\to0}(\Delta\theta/\Delta X)$. Therefore, at the vertical wall we need very fine grids to obtain accurate results. In X-direction, the width of 5 control volumes close to both the vertical boundaries were 1/4 the width of the central control volumes. Also the bottom and top surfaces are assumed adiabatic and impermeable. Therefore in Y-direction, we do not need numerical differentiations. Therefore, the height of 5 control volumes close to both the horizontal boundaries were 1/4 the height of the central control volumes. The discretization equations were solved by the Gauss–Seidel method. The iteration method used in this program is a line-by-line procedure, which is a combination of the direct method and the resulting Tri Diagonal Matrix Algorithm (TDMA). The convergence of the iteration is determined by the change in the average Nusselt and Sherwood numbers as well as other dependent variables through one hundred iterations to be less than 0.01% from its initial value. Fig. 2 shows the convergence and stability of the solution.

4. Program validation and comparison with previous research

In order to check on the accuracy of the numerical technique employed for the solution of the problem considered in the present study, it was validated by performing simulation for double-diffusive convection flow in a vertical rectangular enclosure with combined horizontal temperature and concentration gradients and in the presence of magnetic field and heat generation effects which were reported by Chamkha and Al-Naser [26]. Fig. 3 plots the predicted values for average Nusselt numbers over a range for Hartmann from 0 to 50 for the present solution and the results published by Chamkha and Al-

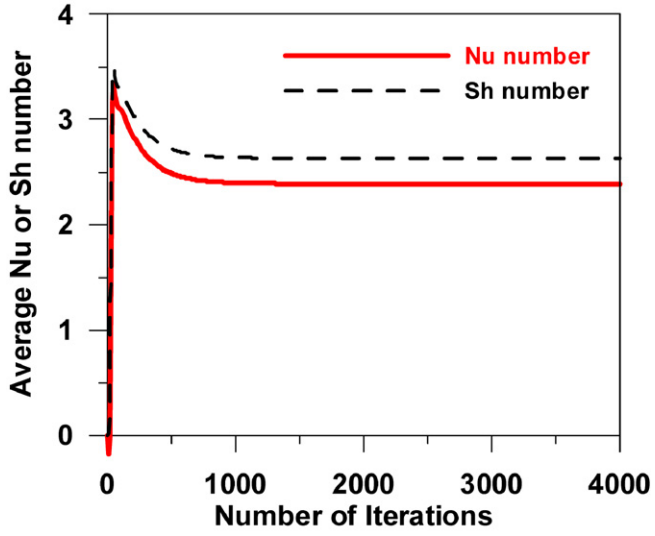

Fig. 2. Convergence and stability of the solution $Ra_T = 10^5$, $N = 1$, $Ha = 50$ and $\phi = 1$.

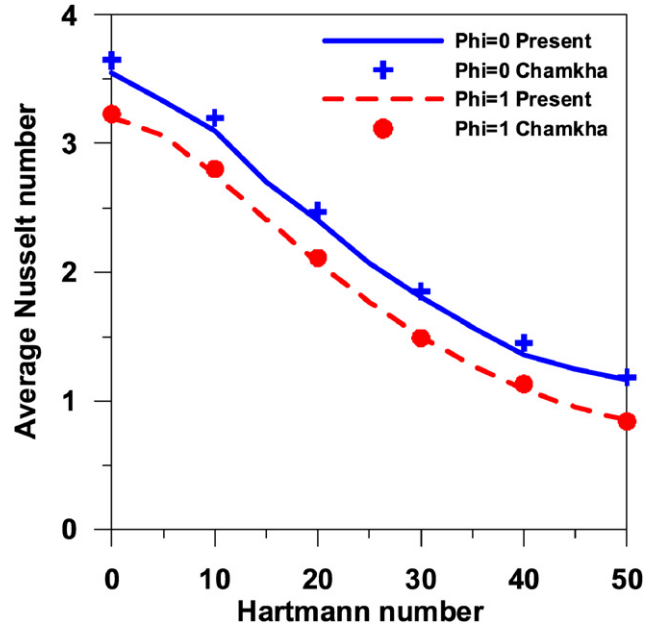

Fig. 3. Comparison for average Nusselt number with Chamkha and Al-Naser [26] results, $N = -0.8$, $Gr_T = 10^5$, $Pr = 1$, $Le = 2$ and $A = 2$.

Naser [26]. In the figure, the heat generation coefficient equals to zero and one. The following parameters were kept constant $N = -0.8$, $Gr_T = 10^5$, $Pr = 1$, $Le = 2$ and $A = 2$. In addition, Fig. 4 plots the values of the average Sherwood number for the same previous conditions. The maximum deviation between the results through this range was within two percent. Some of this deviation may be from the accuracy in the measuring from the graphs or from the solution techniques. Also, Fig. 5(a) and (b) present comparisons for the isotherms, concentration contours, density and streamlines contours of the present work at $N = -0.8$, $Ra_T = 10^5$, $Ha = 25$, $Pr = 1$, $Le = 2$ and $\phi = 0$ and Chamkha and Al-Naser [26]. The figure shows good agreement.

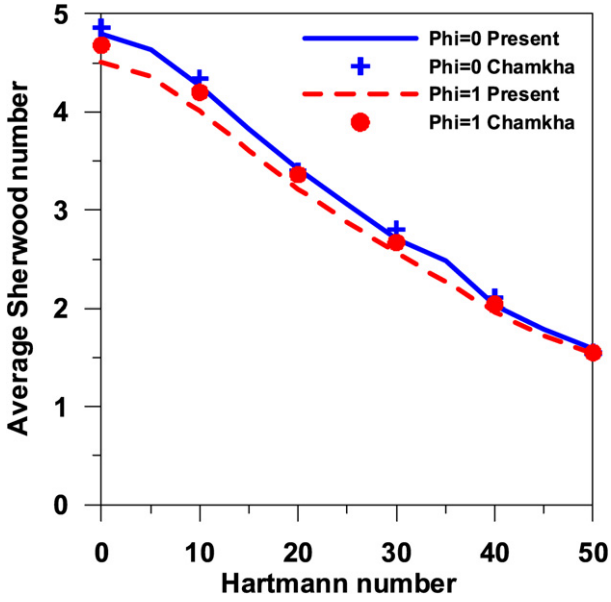

Fig. 4. Comparison for average Sherwood number with Chamkha and Al-Naser [26] results, $N = -0.8$, $Gr_T = 10^5$, $Pr = 1$, $Le = 2$ and $A = 2$.

5. Results and discussion

In this study, the Prandtl number, Pr is kept constant at $Pr = 0.7$, aspect ratio, $A = 2$ and $Le = 1$. The base case in this study is made with thermal Rayleigh number $Ra_T = 10^6$, Hartmann number $Ha = 50$, buoyancy ratio $N = 1$ and dimensionless heat generation $\phi = 1$. The numerical results for the streamline, density, isothermals and isoconcentration contours for various values of thermal Rayleigh number Ra_T, Hartmann number Ha, buoyancy ratio N, and the heat generation or absorption coefficient ϕ, will be presented and discussed. In addition, the results for both average Nusselt, and average Sherwood numbers, at various conditions will be presented and discussed.

Fig. 6 presents the effect of thermal Rayleigh number on the streamline, density, isothermals and isoconcentration contours for Hartmann number $Ha = 50$, $Le = 1$, $Pr = 0.7$, $N = 1$ and $\phi = 1$. In this figure the effect of both thermal buoyancy force and solutal buoyancy force are equal. Therefore, the double diffusive flow is applicable. In addition $\phi = 1$, a heat generation is also considered. For low thermal Rayleigh number $Ra_T = 10^3$, the conduction regime is dominant. The isotherms and isoconcentration are parallel lines. These lines are parallel to the vertical cavity walls. Also, the dimensionless density lines are parallel. The flow consists of a very weak clockwise cell with maximum strength $\Psi_{\max} = 0.1$. Also, it can be seen from the figure an equal spacing separates the isoconcentration lines. On the other hand a non-equal spacing separates the isothermal lines, a wider gab is observed near the hot wall. In ordinary double diffusive flow with out magnetic field nor heat generation nor absorption, the isothermals and isoconcentrations must be similar for $Le = 1$. But in our condition, if a heat source is imposed, it is opposing the heat flow from hot wall. Moreover, the cold wall receives much heat than that input by the hot one. Therefore, near the hot wall, the value of temperature gradient is less than that near the cold wall. As the thermal Rayleigh number is

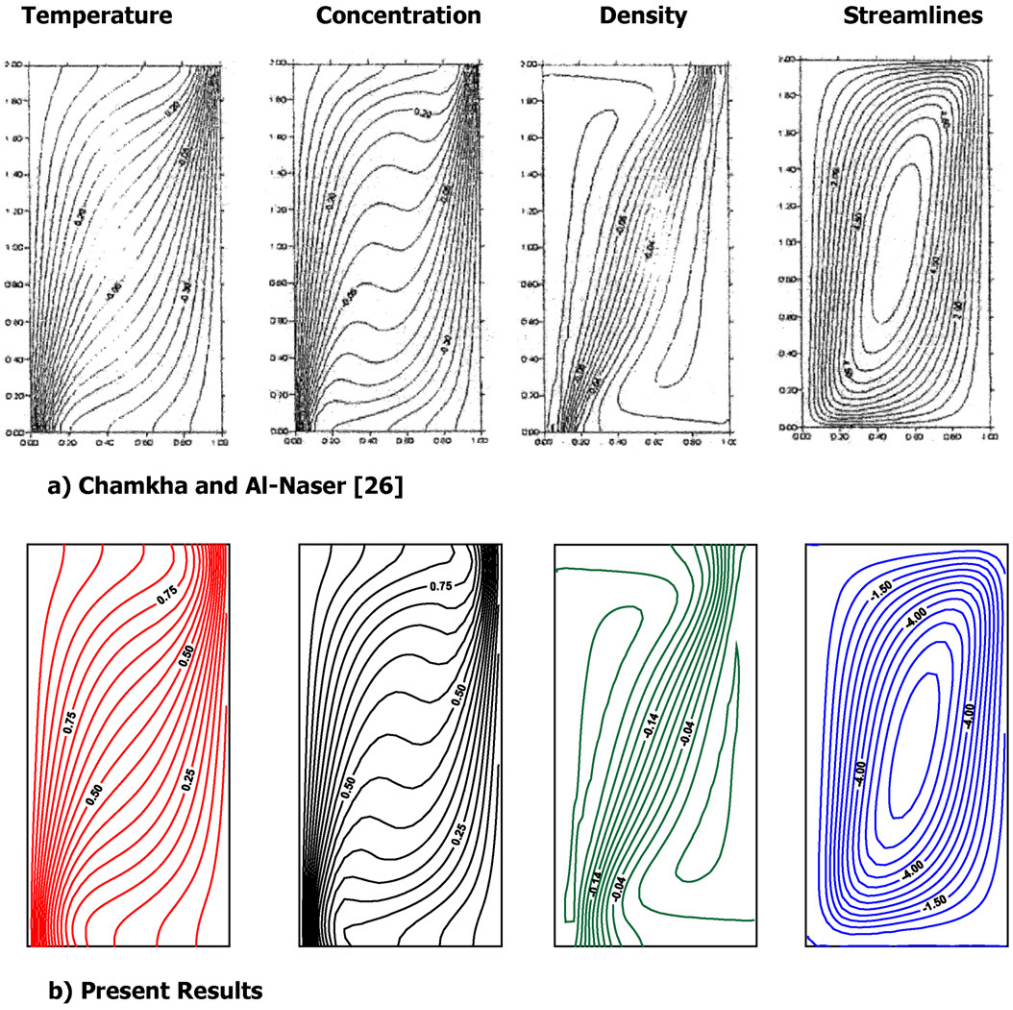

Fig. 5. Comparison with Chamkha and Al-Naser [26], $Ra_T = 10^5$, $Ha = 25$, $Pr = 1$, $Le = 2$ and $\phi = 0$.

increased $Ra_T = 10^4$, the convection mode is pronounced, the flow cell becomes stronger with maximum strength $\Psi_{\max} = 1$. Since, the cell is coming to the hot wall from the cavity bottom and departs from it at the cavity top, both heat and mass transfer at the cavity bottom is higher than at the top. The figure shows, the isothermals and concentrations are closer to the hot wall in the lower region. Furthermore, the effect of heat generation already exists, as mentioned above; the temperature gradient is smaller than the concentration gradient. At thermal Rayleigh number 10^6, the convection is dominant, the circulating cell is very strong with maximum strength $\Psi_{\max} = 24$. The streamlines are crowded near the cavity wall and the cavity core is empty. As well as both isothermals and isoconcentrations are stratified in vertical direction except near the insulated surfaces of the enclosure and appear as horizontal lines in the cavity core. In addition, the heat generation hasn't any significant effect,

Fig. 7 illustrates the effect of Hartmann number Ha, on the streamlines, density, isothermals and isoconcentrations contours. To highlight on the effect of Ha, the thermal Rayleigh number is kept constant $Ra_T = 10^6$, $Pr = 0.7$, $Le = 1$, $N = 1$ and $\phi = 1$. Without magnetic field $Ha = 0$, a very strong clockwise cell is observed as well as the streamlines are very crowded near the vertical walls. Also it is seen horizontal distributions for density, isothermal and concentrations in the cavity core. As the magnetic field is imposed $Ha = 20$, the flow strength slightly reduces and the streamlines penetrates slightly to the cavity core. In addition two small cells appear at the middle cavity height, one in each side. As the Hartmann number increases, the flow strength is damped more, the small cells disappeared, and the streamlines penetrate more towards the cavity center. Consequently, a reduction on the temperature and concentration gradients near the cavity wall and they are tilted upward in the cavity core.

The effect of heat generation or absorption coefficient inside the cavity ϕ, on the different contours is shown in Fig. 8 for $Ra_T = 10^6$, $Pr = 0.7$, $Le = 1$, $N = 1$ and $Ha = 50$. Without heat source or sink $\phi = 0$, the flow is one big central clockwise cell, the flow moves upwards near the hot wall and downwards near the cold one. In addition, the density, isothermals and isoconcentrations are horizontal lines in the cavity core. As heat absorbed is applied $\phi < 0$, according to the conservation of energy law; the rate of heat transfer from the hot wall is higher than the rate of heat received by the cold one. So the fluid

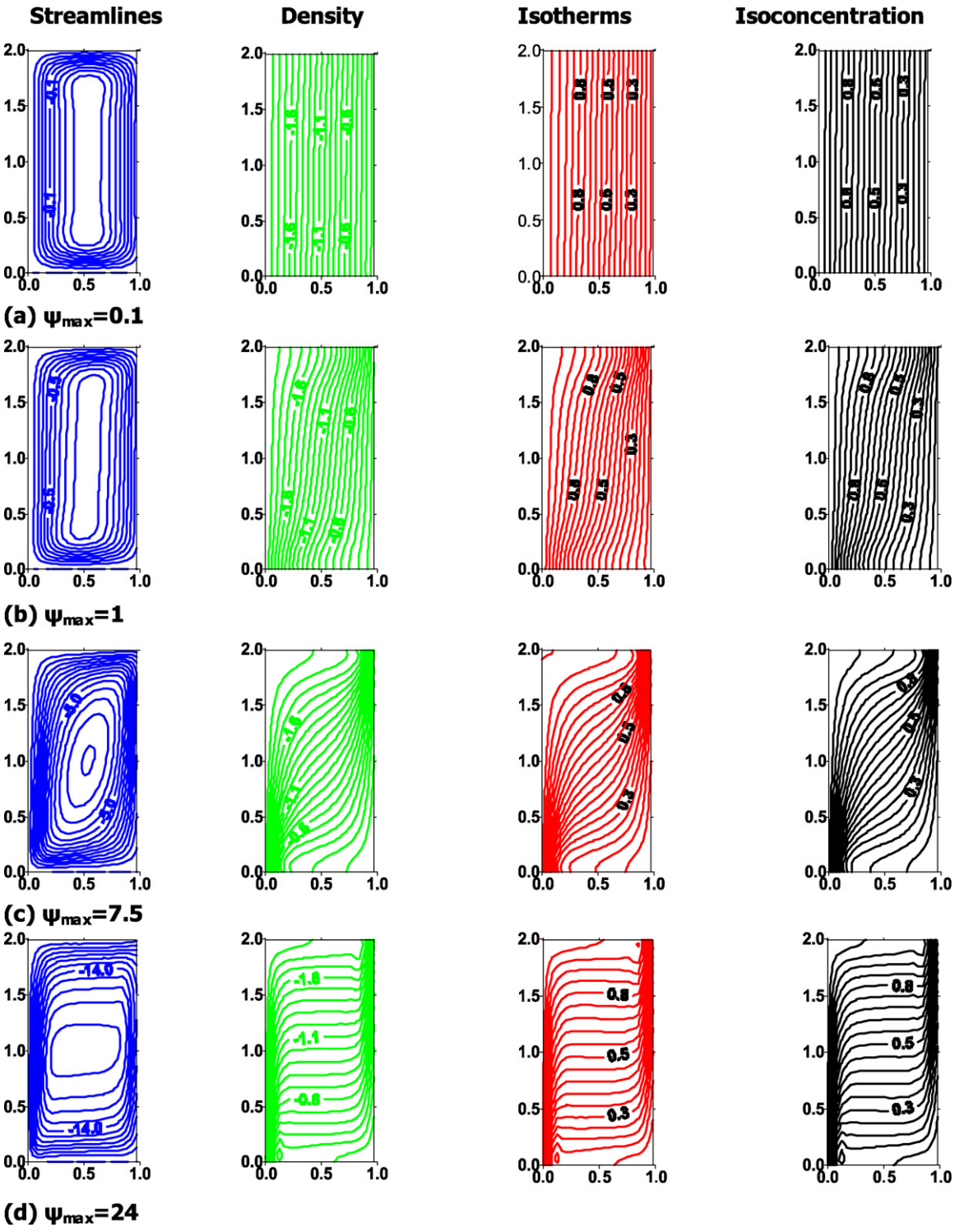

Fig. 6. Streamlines, density, isothermal and isoconcentration contours for $Ha = 50$, $Le = 1$, $N = 1$ and $\phi = 1$ (a) $Ra_T = 10^3$, (b) $Ra_T = 10^4$, (c) $Ra_T = 10^5$, (d) $Ra_T = 10^6$.

velocity near hot wall is higher than that near the cold one. Consequently, the hot wall attracts the cell in the left direction. Furthermore, the temperature gradient increases near the hot wall and the isothermal shifted upwards. As the heat absorption coefficient increases, the cell shifts slightly upwards and more towards to hot wall as well as the isothermals moves upwards. On the other hand, the density contour doesn't change. The heat absorption has a minor effect on the isoconcentrations especially at the upper portion of the cavity, which has a strong flow, the straight lines is destroyed. The presence of heat source within the enclosure $\phi > 0$, causes an increase in the fluid temperature. So the heat transfer from the hot wall is reduced and the heat transfer to the cold is increased. So the cell is shifted right. As the heat generation increases, the fluid temperature

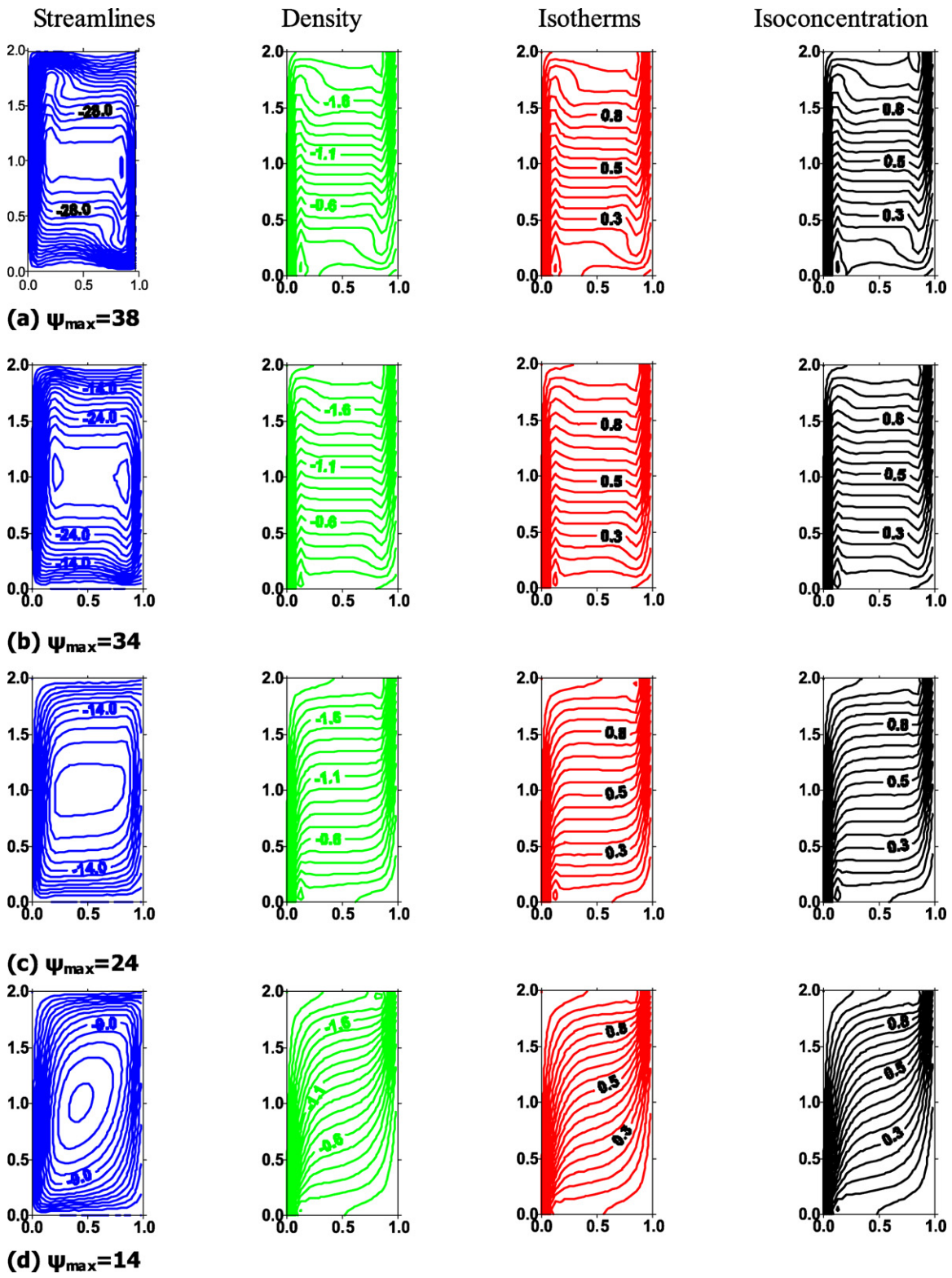

Fig. 7. Streamlines, density, isothermal and isoconcentration contours for $Ra_T = 10^6$, $Le = 1$, $N = 1$ and $\phi = 1$ (a) $Ha = 0$, (b) $Ha = 20$, (c) $Ha = 50$, (d) $Ha = 100$.

increases and reaches more than the hot wall temperature in the upper portion of the cavity. Therefore, the direction of heat transfer reverses and become from the fluid to the hot wall. Consequently, a counterclockwise small cell appeared at the upper left corner. In addition a concentration plume from left lower part is noticed. It is interesting to explore the effect of these phenomena on the distribution for both local Nusselt and Sherwood numbers over the hot wall. Figs. 9 and 10 represent these distributions. In general, the local Nusselt number has maximum values at the cavity bottom and its value decreases as we move

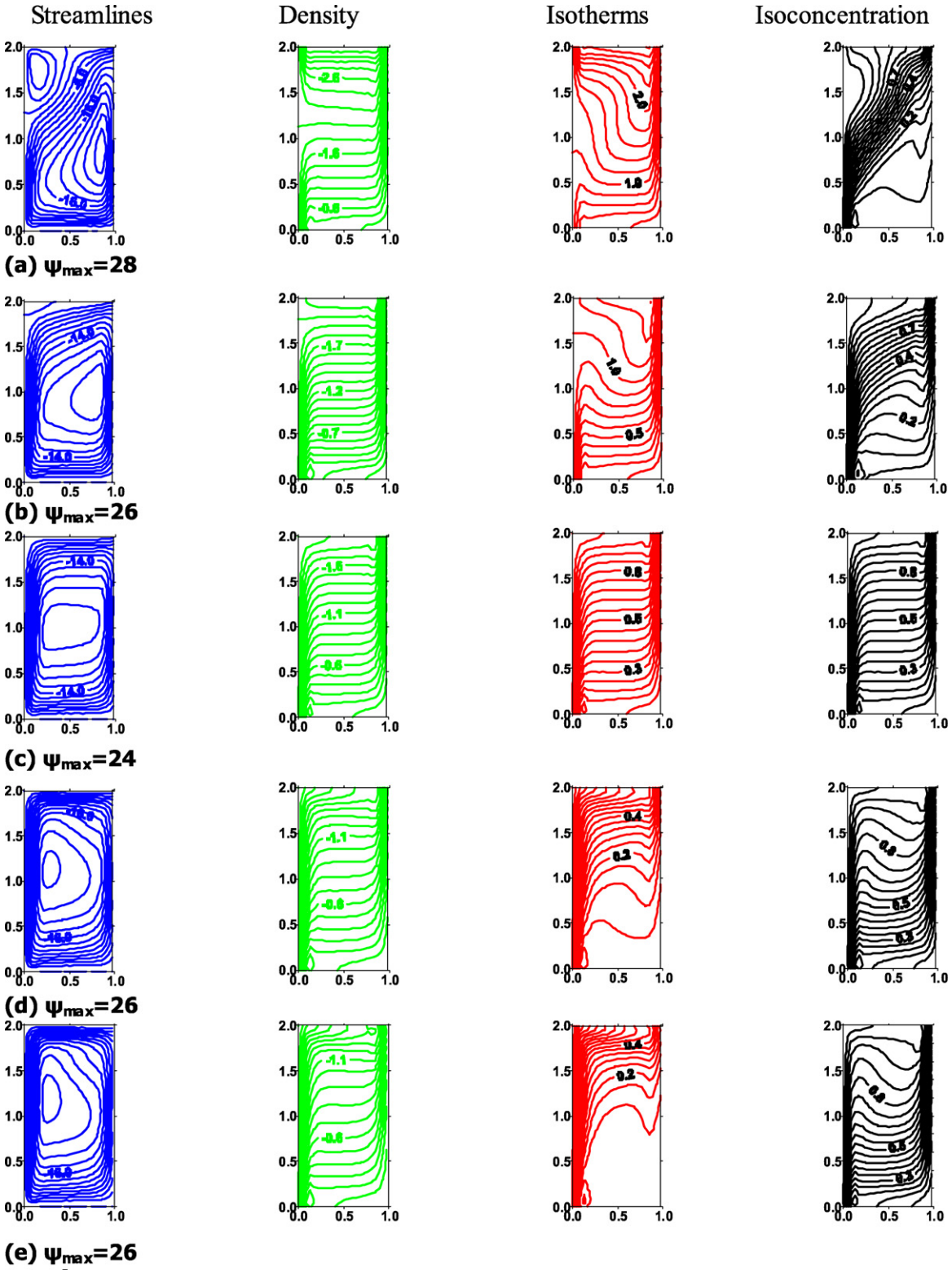

Fig. 8. Streamlines, density, isothermal and isoconcentration contours for $Ra_T = 10^6$, $Le = 1$, $N = 1$ and $Ha = 50$ (a) $\phi = 25$, (b) $\phi = 10$, (c) $\phi = 0$, (d) $\phi = -25$, (e) $\phi = -50$.

upwards. The local Nusselt number decreases as ϕ increases. For strong heat source $\phi = 25$, the local Nusselt has a negative value at the upper section of the cavity. This means that, the heat is transferred from the fluid to the hot wall. The sign of the local Nusselt changes when the small counterclockwise cell appears. If we return to Fig. 8 it is noticeable that the absolute value for the temperature gradient has a maximum value at this position, since this cell is coming to the hot wall at the

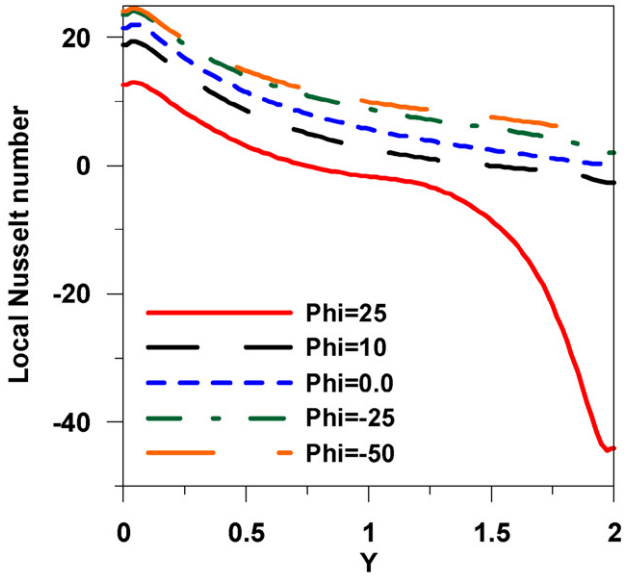

Fig. 9. Effect of heat generation or absorption coefficient ϕ, on local Nusselt number, $Ra_T = 10^6$, $Le = 1$, $N = 1$ and $Ha = 50$.

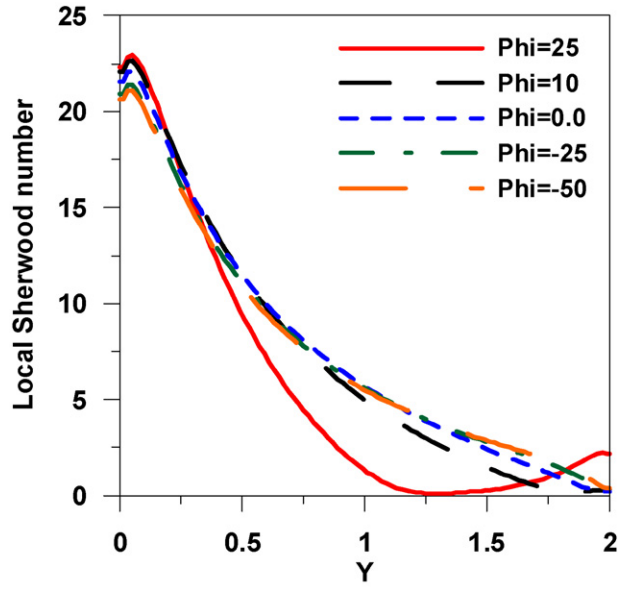

Fig. 10. Effect of heat generation or absorption coefficient ϕ, on local Sherwood number, $Ra_T = 10^6$, $Le = 1$, $N = 1$ and $Ha = 50$.

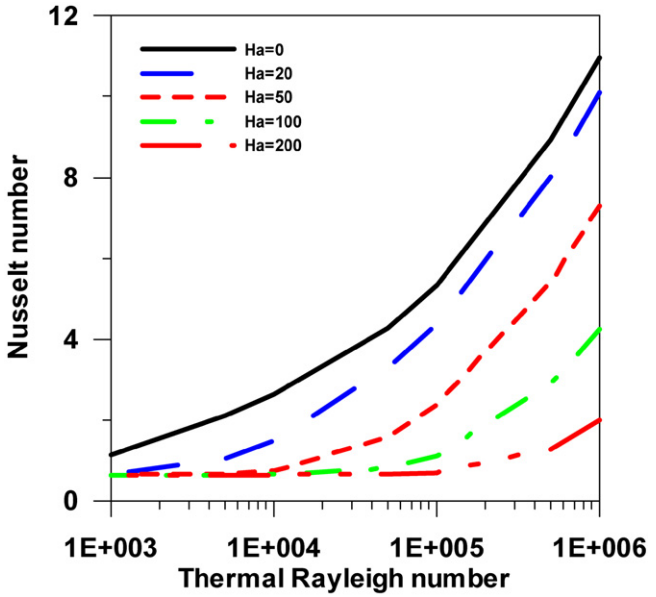

Fig. 11. Nusselt number vs. Ra_T for different Ha, $Le = 1$, $\phi = 1$ and $N = 1$.

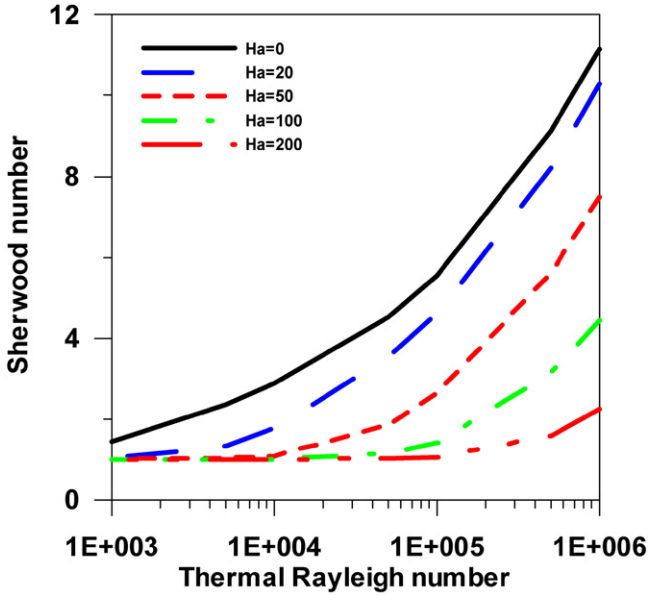

Fig. 12. Sherwood number vs. Ra_T for different Ha, $Le = 1$, $\phi = 1$ and $N = 1$.

upper corner. Consequently, the absolute value for local Nusselt has maximum value. This also can be observed from the high density of the isothermal contours at this section. On the other hand, the heat source or sink have no significant effect on the local Sherwood number.

The combined effect of thermal Rayleigh number and Hartmann number on the average Nusselt and Sherwood numbers is presented in Figs. 11 and 12 for $Le = 1$, $Pr = 0.7$, $\phi = 1$ and $N = 1$. Without imposing the magnetic flux $Ha = 0$, both average Nusselt and Sherwood numbers increases with the thermal Rayleigh number. In addition, for the same value of thermal Rayleigh number, as the magnetic field is increased both average Nusselt and Sherwood numbers decreases. Furthermore, at Hartmann number $Ha > 20$, both the average Nusselt and Sherwood numbers have constant values over a range of thermal Rayleigh number. This range increases with increasing Hartmann number. It is interesting to note that this phenomenon was detected experimentally by Ujihara et al. [1].

The combined effect for the magnetic field and heat source or sink on both average Nusselt and Sherwood numbers is illustrated in Figs. 13 and 14. For constant $Ra_T = 10^6$, $Le = 1$, $Pr = 0.7$ and $N = 1$. It is observed that both Nu and Sh have a decreasing trend with increases in Hartmann number. In addition, it is observed that heat generation ($\phi > 0$) decreases the average Nusselt number while heat absorption ($\phi < 0$) increases it. However, heat generation ($\phi > 0$) and heat absorption ($\phi < 0$), slightly decrease the average Sherwood number.

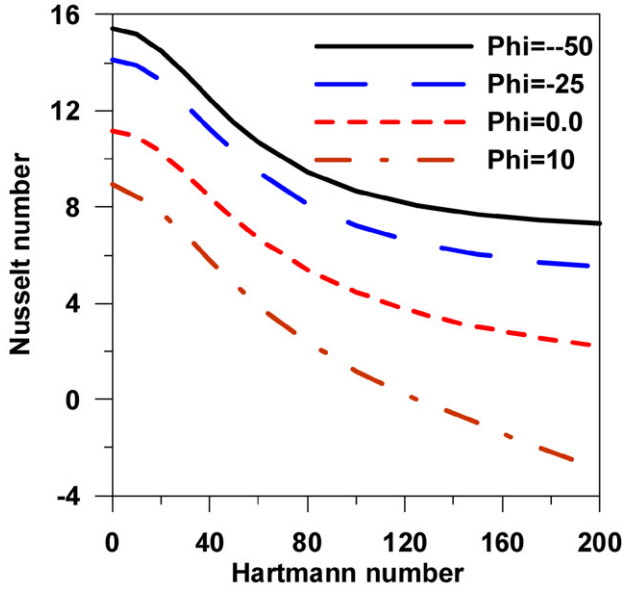

Fig. 13. Nusselt number vs. Hartmann number for different ϕ, $Ra_T = 10^6$, $Le = 1$ and $N = 1$.

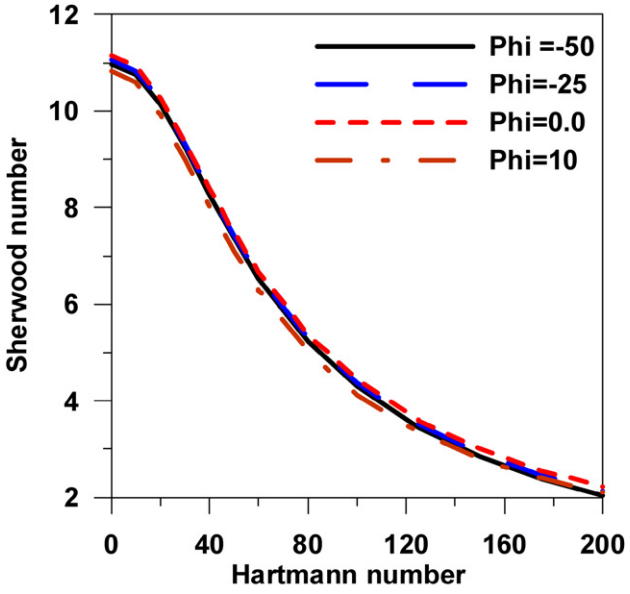

Fig. 14. Sherwood number vs. Hartmann number for different ϕ, $Ra_T = 10^6$, $Le = 1$ and $N = 1$.

As expected, the effect of the heat generation or absorption coefficient ϕ is more pronounced on the values of Nusselt than on Sherwood. Moreover, for heat source with high coefficient, the sign of the average Nusselt number is changed from positive to negative.

The influence of the buoyancy ratio N on the average Nusselt and Sherwood numbers for different Hartmann number is shown in Figs. 15 and 16, respectively, for $Ra_T = 10^6$, $Le = 1$ and $\phi = 1$. It is interesting to observe from these figures the existence of minimum values in both average Nusselt and Sherwood numbers for a buoyancy ratio of about -1. The values of Nu and Sh tend to increase with increasing the absolute values

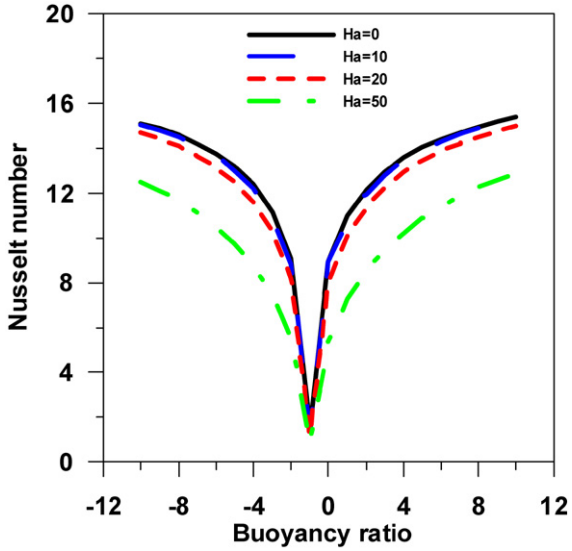

Fig. 15. Average Nusselt number vs. buoyancy ratio for different Hartmann numbers, $Ra_T = 10^6$, $Le = 1$ and $\phi = 1$.

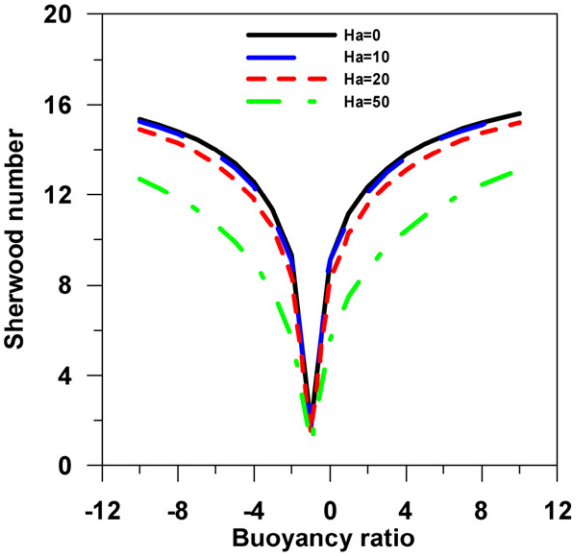

Fig. 16. Average Sherwood number vs. buoyancy ratio for different Hartmann numbers, $Ra_T = 10^6$, $Le = 1$ and $\phi = 1$.

of Buoyancy ratio. The existence of such minimum values in Nusselt and Sherwood has been reported in the literature.

6. Conclusions

Steady heat and mass transfer by natural convection flow of a heat generating fluid inside a rectangular enclosure in the presence of a transverse magnetic field was studied numerically. The finite-difference method was employed for the solution of the present problem. Comparisons with previously published work on special cases of the problem were performed and found to be in good agreement. Graphical results for various parametric conditions were presented and discussed. The study revealed the following:

The heat and mass transfer mechanisms and the flow characteristics inside the enclosure depended strongly on the strength of the magnetic field and heat generation or absorption effects. The magnetic field was found to reduce the heat transfer and fluid circulation within the enclosure.

The average Nusselt number was increased in the presence of a heat sink while it was decreased when a heat source was present. The sign of the average Nusselt number was changed from positive to negative in the case of high heat generation.

The presence of heat source or heat sink slightly reduces the average Sherwood number. For Hartmann number $Ha > 20$, both the average Nusselt and Sherwood numbers have constant values over a range of thermal Rayleigh number, this range increases with increasing Hartmann number. Finally the average Nusselt and Sherwood numbers have minimum values at buoyancy ratio $N = 1$.

References

[1] A. Ujihara, T. Tagawa, H. Ozoe, Average heat transfer rates measured in two different temperature ranges for magnetic convection of horizontal water layer heated from below, Int. J. Heat Mass Transfer 49 (2006) 3555–3560.

[2] S. Ostrach, Natural convection with combined driving forces, Phys. Chem. Hydrodyn. 1 (1980) 233–247.

[3] S. Acharya, R.J. Goldstein, Natural convection in an externally heated square box containing internal energy sources, J. Heat Transfer 107 (1985) 855–866.

[4] M. Rahman, M.A.R. Sharif, Numerical study of laminar natural convection in inclined rectangular enclosures of various aspect ratios, Numer. Heat Transfer A 44 (2003) 355–373.

[5] H. Oztop, E. Bilgen, Natural convection in differentially heated and partially divided square cavities with internal heat generation, Int. J. Heat Fluid Flow 27 (2006) 466–475.

[6] S.V. Patankar, Numerical Heat Transfer and Fluid Flow, McGraw-Hill, New York, 1980.

[7] Y. Shu, B.Q. Li, H.C. de Groh, Magnetic damping of g-jitter induced double-diffusion convection, Numer. Heat Transfer A 42 (2002) 345–364.

[8] H. Ozoe, K. Okada, The effect of the direction of the external magnetic field on the three-dimensional natural convection in a cubic enclosure, Int. J. Heat Mass Transfer 32 (1989) 1939–1953.

[9] T. Alboussière, J.P. Garandet, R. Moreau, Asymptotic analysis and symmetry in MHD convection, Phys. Fluids 8 (1996) 2215–2226.

[10] N.I. Wakayama, Behavior of flow under gradient magnetic field, J. Appl. Phys. 69 (4) (1991) 2734–2736.

[11] B. Bai, A. Yabe, J. Qi, N.I. Wakayama, Quantitative analysis of air convection caused by magnetic–fluid coupling, AIAA J. 37 (1999) 1538–1543.

[12] T. Tagawa, R. Shigemitsu, H. Ozoe, Magnetizing force modeled and numerically solved for natural convection of air in a cubic enclosure: effect of the direction of the magnetic field, Int. J. Heat Mass Transfer 45 (2002) 267–277.

[13] M. Kaneda, T. Tagawa, H. Ozoe, Convection induced by a cusp-shaped magnetic field for air in a cube heated from above and cooled from below, J. Heat Transfer 124 (2002) 17–25.

[14] B. Xu, B.Q. Li, D.E. Stock, An experimental study of thermally induced convection of molten gallium in magnetic fields, Int. J. Heat Mass Transfer 49 (2006) 2009–2019.

[15] J.L. Morton, N. Ma, D.F. Bliss, G.G. Bryant, Dopant segregation during liquid-encapsulated Czochralski crystal growth in a steady axial magnetic field, J. Crystal Growth 242 (2002) 471–485.

[16] N. Ma, J.S. Walker, A model of dopant transport during Bridgman crystal growth with magnetically damped buoyant convection, J. Heat Transfer 122 (2000) 159–164.

[17] N. Ma, J.S. Walker, A parametric study of segregation effects during vertical Bridgman crystal growth with an axial magnetic field, J. Crystal Growth 208 (2000) 757–771.

[18] J.F. Kuniholm, N. Ma, Natural convection in a liquid encapsulated molten semiconductor with a steady magnetic field, Int. J. Heat Fluid Flow 24 (2003) 130–136.

[19] M. Yang, N. Ma, A computational study of natural convection in a liquid-encapsulated molten semiconductor with a horizontal magnetic field, Int. J. Heat Fluid Flow 26 (2005) 810–816.

[20] X. Wang, N. Ma, D.F. Bliss, G.W. Iseler, P. Becla, Comparing modified vertical gradient freezing with rotating magnetic fields or with steady magnetic and electric fields, J. Crystal Growth 287 (2006) 270–274.

[21] X. Wang, N. Ma, D.F. Bliss, G.W. Iseler, Semiconductor crystal growth by modified vertical gradient freezing with electromagnetic stirring, J. Thermophys. Heat Transfer 19 (2005) 95–100.

[22] A.M. Holmes, X. Wang, N. Ma, D.F. Bliss, G.W. Iseler, Vertical gradient freezing using submerged heater growth with rotation and with weak magnetic and electric fields, Int. J. Heat Fluid Flow 26 (2005) 792–800.

[23] X. Wang, N. Ma, D.F. Bliss, G.W. Iseler, A numerical investigation of dopant segregation by modified vertical gradient freezing with moderate magnetic and weak electric fields, Int. J. Engrg. Sci. 43 (2005) 908–924.

[24] X. Wang, N. Ma, D.F. Bliss, G.W. Iseler, Solute segregation during modified vertical gradient freezing of alloyed compound semiconductor crystals with magnetic and electric fields, Int. J. Heat Mass Transfer 49 (2006) 3429–3438.

[25] T. Nishimura, M. Wakamatsu, A.M. Morega, Oscillatory double-diffusive convection in a rectangular enclosure with combined horizontal temperature and concentration gradients, Int. J. Heat Mass Transfer 41 (1998) 1601–1611.

[26] A.J. Chamkha, H. Al-Naser, Hydromagnetic double-diffusive convection in a rectangular enclosure with opposing temperature and concentration gradients, Int. J. Heat Mass Transfer 45 (2002) 2465–2483.

[27] A.J. Chamkha, H. Al-Naser, Hydromagnetic double-diffusive convection in a rectangular enclosure with uniform side heat and mass fluxes and opposing temperature and concentration gradients, Int. J. Thermal Sci. 41 (2002) 936–948.